Click Here for Full Article

Interannual variations in continental-scale net carbon exchange and sensitivity to observing networks estimated from atmospheric CO_2 inversions for the period 1980 to 2005

Kevin R. Gurney,[1] David Baker,[2] Peter Rayner,[3] and Scott Denning[4]

[1] Interannually varying net carbon exchange fluxes from the TransCom 3 Level 2 Atmospheric Inversion Intercomparison Experiment are presented for the 1980 to 2005 time period. The fluxes represent the model mean, net carbon exchange for 11 land and 11 ocean regions after subtraction of fossil fuel CO_2 emissions. Both aggregated regional totals and the individual regional estimates are accompanied by a model uncertainty and model spread. We find that interannual variability is larger on the land than the ocean, with total land exchange correlated to the timing of both El Niño/Southern Oscillation (ENSO) as well as the eruption of Mt. Pinatubo. The post-Pinatubo negative flux anomaly is evident across much of the tropical and northern extratropical land regions. In the oceans, the tropics tend to exhibit the greatest level of interannual variability, while on land, the interannual variability is slightly greater in the tropics and northern extratropics. The interannual variation in carbon flux estimates aggregated by land and ocean across latitudinal bands remains consistent across eight different CO_2 observing networks. The interannual variation in carbon flux estimates for individual flux regions remains mostly consistent across the individual observing networks. At all scales, there is considerable consistency in the interannual variations among the 13 participating model groups. Finally, consistent with other studies using different techniques, we find a considerable positive net carbon flux anomaly in the tropical land during the period of the large ENSO in 1997/1998 which is evident in the Tropical Asia, Temperate Asia, Northern African, and Southern Africa land regions. Negative anomalies are estimated for the East Pacific Ocean and South Pacific Ocean regions. Earlier ENSO events of the 1980s are most evident in southern land positive flux anomalies.

Citation: Gurney, K. R., D. Baker, P. Rayner, and S. Denning (2008), Interannual variations in continental-scale net carbon exchange and sensitivity to observing networks estimated from atmospheric CO_2 inversions for the period 1980 to 2005, *Global Biogeochem. Cycles*, *22*, GB3025, doi:10.1029/2007GB003082.

1. Introduction

[2] The fate of CO_2 emitted into the atmosphere from the combustion of fossil fuels, industrial processes, changes in vegetation, and ocean processes remains a topic of active scientific research, not to mention being of great significance to the climate change policy community. Studies based on observations of atmospheric CO_2 combined with estimates of global fossil/industrial and deforestation emissions have concluded that the land and oceans are removing roughly half of the anthropogenic CO_2 input [*Prentice et al.*, 2001]. Also evident is the considerable variation in this uptake from 1 year to the next [*Baker et al.*, 2006]. Though a number of hypotheses have been suggested to explain the long-term and interannual variations, direct confirmation of these mechanisms at the regional to global scale remains elusive.

[3] The importance of an improved understanding of carbon exchange has emerged as a key research priority. This has been underscored by research showing a large spread of projected future warming when global carbon cycle models are coupled to simulations of climate change [*Friedlingstein et al.*, 2006]. While some simulations show the ocean and land continuing as a carbon sink, others show the biosphere undergoing dramatic changes. For example, coupled simulations from the Hadley Center in the UK suggest a future in which the American tropical forests undergo significant dieback from increased water stress in addition to widespread oxidation of soil carbon [*Cox et al.*, 2000].

[1] Department of Earth and Atmospheric Sciences/Department of Agronomy, Purdue University, West Lafayette, Indiana, USA.
[2] Woods Hole Oceanographic Institution, Woods Hole, Massachusetts, USA.
[3] LSCE-CEA de Saclay, Orme des Merisiers, Gif/Yvette, France.
[4] Department of Atmospheric Science, Colorado State University, Fort Collins, Colorado, USA.

[4] Efforts to understand the current exchange of carbon between the land, oceans, and atmosphere have included a number of observing techniques and simulation approaches. One approach that has met with increasing use is the atmospheric inversion approach, in which the spatial and temporal pattern of atmospheric CO_2 observations is used in combination with simulated atmospheric transport to infer sources and sinks of CO_2 at the surface [*Enting*, 2002].

[5] In the last two decades, a number of research groups around the world have carried out atmospheric inversion experiments in an effort to quantify CO_2 sources and sinks at a variety of spatial and temporal scales. These began with efforts to estimate the long-term mean exchange at large scales, and have more recently focused on interannual variability and attempts to estimate fluxes at smaller scales [*Enting et al.*, 1995; *Fan et al.*, 1998; *Bousquet et al.*, 2000; *Rayner et al.*, 1999a; *Gurney et al.*, 2002; *Rödenbeck et al.*, 2003b; *Peylin et al.*, 2005; *Baker et al.*, 2006]. Though there is some agreement regarding the hemispheric estimates of carbon exchange, quantification at the continental and regional scale remains particularly uncertain. The spread in the estimates of continental-scale carbon exchange can be traced to a few aspects of the inverse approach: the paucity of CO_2 observational data and methods for addressing this, the transport simulation employed, and the inversion conditioning and setup [*Engelen et al.*, 2002].

[6] In the 1990s an experiment was constructed to intercompare the many transport models and data used in atmospheric CO_2 inversion studies in an effort to better understand the sources of uncertainty and potentially arrive at a consensus view of net carbon uptake in the land and oceans. The TransCom experiment contained a number of incremental steps, starting with forward simulations of fossil fuel CO_2, net biosphere exchange, and sulfur hexafluoride. The most recent phase of the TransCom experiment is the TransCom 3 effort. TransCom 3 gathered the forward CO_2 sensitivities of the participating modeling groups and explored the uncertainties arising in the inversion process from the transport, the data and the inversion set-up itself [*Gurney et al.*, 2000].

[7] A number of papers have been written highlighting analysis of the TransCom 3 results, including an annual mean inversion [*Gurney et al.*, 2002, 2003], a cyclostationary or seasonal inversion [*Gurney et al.*, 2004] and an interannual inversion [*Baker et al.*, 2006]. In addition, a number of sensitivity studies have been presented, examining particular aspects of the TransCom atmospheric inversion including data uncertainties [*Law et al.*, 2003], uncertainties in the fossil fuel CO_2 data [*Gurney et al.*, 2005], extension of the observing network [*Patra et al.*, 2003], an examination of ocean-only observing networks [*Patra et al.*, 2006], an exploration of the error terms [*Engelen et al.*, 2002], and a comparison to vertical profile observations [*Stephens et al.*, 2007].

[8] The current study builds from the work of *Baker et al.* [2006] in which an interannual inversion was performed for the 1988 to 2003 time period using all of the TransCom 3, level 2 models. The focus of that study was on the presentation of a "control" or "typical" inversion setup and the flux results and the associated model-dependent uncertainties. Here, we extend the time period of interest to cover 1980 to 2005, allowing for examination of two prominent ENSO events in the 1980s. Most importantly, we build a series of CO_2 observing networks for different subsets of our 27-year time span that progressively contain larger numbers of observing stations, allowing for constant observational constraints in the inversion for spans of different lengths [*Rödenbeck et al.*, 2003b; *Peylin et al.*, 2005]. The distinct contribution of this work is the ability to test the sensitivity of station network choices, while accounting for transport uncertainties using a 13 model portfolio, in determining the net carbon variability of 1 year to the next.

[9] Section 2 of this paper provides an explanation of our methods and how the current study differs methodologically from the work of *Baker et al.* [2006]. In section 3, we present the results of the interannual inversion, using on the mean of the thirteen participating model groups. We present the interannual variability by detrending and deseasonalizing the net carbon exchange in each of the 22 regions, and in grouping the results in a series of progressively larger regions for which the estimation confidence is greater. Both types of estimation error generated in the TransCom experiment are included in all results. This section also presents the estimated carbon exchange given using measurements from different observing networks spanning different subperiods in the 27-year timespan. In section 4 we discuss the large, coherent cross-network variations, emphasizing the relationship to the El Niño/Southern Oscillation (ENSO). In section 5 we summarize these results and point toward further analysis and the next steps that the TransCom community is taking to further refine and explore atmospheric CO_2 inversion research.

2. Methods

2.1. Formalism and Design

[10] The inversion approach used in this study follows the Bayesian synthesis method [*Tarantola*, 1987; *Enting*, 2002]. The goal of the atmospheric inversion process is to find the optimal combination of regional surface net carbon fluxes, $\vec{S}$, that best matches observed CO_2, $\vec{D}$, after those fluxes have been transported through a model atmosphere represented by the operator, M. This is most succinctly represented by the minimization of cost function, J:

$$J = \frac{1}{2}\left[\left(\mathbf{M}\vec{S} - \vec{D}\right)^T \mathbf{C}(\vec{D})^{-1}\left(\mathbf{M}\vec{S} - \vec{D}\right) \\ + \left(\vec{S} - \vec{S}_0\right)^T \mathbf{C}\left(\vec{S}_0\right)^{-1}\left(\vec{S} - \vec{S}_0\right)\right] \tag{1}$$

where $\mathbf{C}(\vec{D})$ is the covariance matrix assumed to represent mismatches between the modeled and observed concentrations, and $\mathbf{C}(\vec{S})$ is the covariance matrix representing uncertainties in the prior fluxes. A detailed description of the formalism employed and references to source material are given in previous work for the annual mean [*Gurney et al.*, 2003] and interannual "control" [*Baker et al.*, 2006] TransCom 3 inversions.

[11] Details of the experimental design can be similarly found in the TransCom 3 experimental protocol [*Gurney et al.*, 2000] and the previous TransCom 3 results [*Baker et al.*, 2006; *Gurney et al.*, 2003]. The results presented here follow the inversion set-up outlined in the control interannual inversion [*Baker et al.*, 2006]. The following is a brief summary.

[12] Thirteen transport models (or model variants) ran a series of forward CO_2 tracer simulations in order to construct model-specific response functions of atmospheric CO_2. The thirteen transports models are described in *Baker et al.* [2006] Table 2.

[13] For the interannual inversion experiment presented here, the forward simulations were run as Green's functions. A total of 268 tracers were simulated by each model, four of which were "background" global fluxes and 264 of which were region/month fluxes representing a combination of 12 months and the 22 land and ocean regions described in the annual mean inversion experiment [*Gurney et al.*, 2002]. The prespecified background flux patterns were emitted for a single year, then discontinued, allowing the CO_2 concentration field to decay for the following 2 years of simulation. The prespecified region/month flux patterns were emitted for a single month then discontinued for the remainder of the 3-year simulation.

[14] In order to lower the computational burden for the participating modeling groups, interannually varying transport was not required. Participants chose a variety of different annually repeating transport products encompassing reanalyzed winds and GCM transport simulations. The lack of interannual transport in the forward simulations is an important consideration in the flux estimation. Four studies have tested the influence of interannual transport versus repeated annual transport fields and the results remain somewhat inconclusive. [*Dargaville et al.*, 2000; *Rödenbeck et al.*, 2003a; P. Patra, personal communication, April 2005; *Peylin et al.*, 2005]. When examining latitudinal aggregates ($90-30°S$, $30-0°S$, $0-30°N$, $30-90°N$) for fixed versus interannually-varying winds, *Dargaville et al.* [2000] found that the predominant difference was in the flux amplitude as opposed to the phasing of the interannual variations. By contrast, *Rödenbeck et al.* [2003a] found both amplitude and phase flux differences when comparing interannually varying winds to a series of fixed-year transport winds, though the phasing differences were found mostly in the northern temperate zone ($15-50°N$). In this region, flux differences occasionally exceeded 1.0 GtC/year. Finally, the work of *Peylin et al.* [2005] indicates that the main impact of interannually varying winds is on the amplitude as opposed to the phasing of the carbon flux and these effects are evident at the regional scale only. As described in *Baker et al.* [2006], recent unpublished inverse-estimated fluxes show small standard errors of roughly 0.2 GtC/year result from computations run with fixed versus interannually varying winds [P. Patra, personal communication, April 2005]. However, it is important to note that though each group used a single year of winds which were repeated to build the CO_2 response functions, many of the modeling groups employed different repeating calendar years in their simulations. Thus the spread in the model results

not only reflects different transport algorithms but a mix of the individual year chosen for the recycled winds. Nevertheless, the lack of interannually varying transport must be considered when interpreting the interannual flux variations.

[15] The four background carbon fluxes consisted of 1990 and 1995 fossil fuel emission fields, an annually-balanced, seasonal biosphere exchange and air-sea gas exchange [*Andres et al.*, 1996; *Brenkert*, 1998; *Randerson et al.*, 1997; *Takahashi et al.*, 1999]. These fluxes are included in the inversion with a small prior uncertainty ($\mathbf{C}(\vec{S_0})$ in equation (1)) so that their magnitude is effectively fixed. Examination and implication of these background fluxes have been explored in previous work [*Gurney et al.*, 2003, 2005]. The 264 region/month fluxes estimated by the inversion are deviations from these global background fluxes for each month in each year and are given prior flux uncertainties of a much larger magnitude than the background fluxes, allowing for significant adjustment given the dictates of the CO_2 observations. The background fossil fuel emission fluxes were prescribed without seasonality. The neutral terrestrial fluxes were purely seasonal (i.e., they integrate to zero across the full year), and the background ocean fluxes were prescribed with both seasonal variations and annual mean uptake.

[16] The same seasonally-varying prior fluxes used in the cyclostationary inversion study [*Gurney et al.*, 2004] were used here. The prior flux uncertainty is important for keeping the estimated fluxes within biogeochemically realistic bounds, though the inclusion of prior fluxes can strongly influence the estimated flux where observations are limited. The extent of this influence depends on the prior flux uncertainty, which has been explored in previous TransCom work. The prior flux uncertainties used in the main diagonal of the prior flux covariance matrix are identical to those used in the cyclostationary control inversion [*Gurney et al.*, 2004] for land, while the regional ocean prior flux uncertainties for each month are a constant value defined as

$$\mathbf{C}(S_{ocn}) = \sqrt{(0.50 \, \text{GtC/yr})^2 + \left[\mathbf{C}\left(S_{L1, ocn}\right)\right]^2} \qquad (2)$$

where $C(S_{\text{L1,ocn}})$ are the annual mean prior flux uncertainties used in the annual mean control inversion [*Gurney et al.*, 2002].

[17] The CO_2 observational data were derived from the GLOBALVIEW-2006 data set [*GLOBALVIEW-CO2*, 2006]. GLOBALVIEW is a data product that interpolates flask and continuous CO_2 measurements to give 48 synchronous values per year. Gaps in the data are filled by extrapolation from marine boundary layer measurements. Because many of the stations within the observational data set have been initiated/retired at various times over the last quarter century and significant gaps exist, a number of different station networks were constructed in this experiment and used to create independent interannual flux estimates. Including or retiring observing sites in a continuous fashion with one network construction can introduce false variability at the

Table 1. Site Number, Time Period, Station Count, and Individual Station Code Names[a] for the Eight Networks Considered in This Study[b]

Site #	80-05 / 24	80-97 / 27	80-90 / 30	90-05 / 57	90-99 / 75	93-05 / 89	95-05 / 95	95-01 / 102
1	alt_06D0	alt_06D0	alt_06D0	alt_01D0	aia005_02D2	alt_01D0	alt_01D0	alt_01D0
2	ams_11C0	ams_11C0	ams_01D0	alt_02D0	aia015_02D2	alt_02D0	alt_02D0	alt_02D0
3	asc_01D0	asc_01D0	ams_11C0	alt_06C0	aia025_02D2	alt_06C0	alt_06C0	alt_04D0
4	azr_01D0	azr_01D0	asc_01D0	alt_06D0	aia045_02D2	alt_06D0	alt_06D0	alt_06C0
5	brw_01C0	bhd_15C0	avi_01D0	ams_11C0	alt_01D0	ams_11C0	ams_11C0	alt_06D0
6	brw_01D0	brw_01C0	azr_01D0	asc_01D0	alt_02D0	asc_01D0	asc_01D0	ams_11C0
7	cba_01D0	brw_01D0	bhd_15C0	bme_01D0	alt_04D0	azr_01D0	ask_01D0	asc_01D0
8	cmn_17C0	cba_01D0	brw_01C0	bmw_01D0	alt_06C0	bal_01D1	azr_01D0	ask_01D0
9	gmi_01D0	cmn_17C0	brw_01D0	brw_01C0	alt_06D0	bme_01D0	bal_01D1	azr_01D0
10	key_01D0	cmo_01D0	cba_01D0	brw_01D0	ams_11C0	bmw_01D0	bme_01D0	bal_01D1
11	kum_01D0	gmi_01D0	cmn_17C0	cfa_02D0	asc_01D0	brw_01C0	bmw_01D0	bhd_15C0
12	mlo_01C0	key_01D0	cmo_01D0	cgo_01D0	bhd_15C0	brw_01D0	brw_01C0	bme_01D0
13	mlo_01D0	kum_01D0	gmi_01D0	cgo_02D0	bme_01D0	bsc_01D0	brw_01D0	bmw_01D0
14	nwr_01D0	mbc_01D0	key_01D0	cmn_17C0	bmw_01D0	car030_01D2	bsc_01D0	brw_01C0
15	psa_01D0	mlo_01C0	kum_01D0	crz_01D0	brw_01C0	car040_01D2	car030_01D2	brw_01D0
16	sch_23C0	mlo_01D0	mbc_01D0	esp_06D0	brw_01D0	car050_01D2	car040_01D2	bsc_01D0
17	sey_01D0	nwr_01D0	mlo_01C0	frd040_06C3	cba_01D0	car060_01D2	car050_01D2	car030_01D2
18	smo_01C0	psa_01D0	mlo_01D0	gmi_01D0	cfa_02D0	cfa_02D0	car060_01D2	car040_01D2
19	smo_01D0	sch_23C0	nwr_01D0	gsn_24D0	cgo_01D0	cgo_01D0	cfa_02D0	car050_01D2
20	spo_01C0	sey_01D0	psa_01D0	hba_01D0	cgo_02D0	cgo_02D0	cgo_01D0	car060_01D2
21	spo_01D0	smo_01C0	sbl_06D0	izo_01D0	cgo_04D0	cmn_17C0	cgo_02D0	cba_04D0
22	stm_01D0	smo_01D0	sch_23C0	key_01D0	cmn_17C0	cpt_36C0	cmn_17C0	cfa_02D0
23	stmebc_01D0	spo_01C0	sey_01D0	kum_01D0	crz_01D0	crz_01D0	coi_20C0	cgo_01D0
24	wes_23C0	spo_01D0	smo_01C0	maa_02D0	frd040_06C3	eic_01D0	cpt_36C0	cgo_02D0
25		stm_01D0	smo_01D0	mhd_01D0	gmi_01D0	esp_06D0	crz_01D0	cgo_04D0
26		stmebc_01D0	spo_01C0	mid_01D0	gsn_24D0	frd040_06C3	eic_01D0	cmn_17C0
27		wes_23C0	spo_01D0	mlo_01C0	hba_01D0	gmi_01D0	esp_06D0	coi_20C0
28			stm_01D0	mlo_01D0	itn051_01C3	gsn_24D0	frd040_06C3	cpt_36C0
29			stmebc_01D0	mlo_02D0	itn496_01C3	hat_20C0	gmi_01D0	cri_02D0
30			wes_23C0	mqa_02D0	izo_01D0	hba_01D0	gsn_24D0	crz_01D0
31				nwr_01D0	izo_27C0	hun_01D0	hat_20C0	eic_01D0
32				poc000_01D1	key_01D0	hun082_35C3	hba_01D0	esp_02D0
33				pocn05_01D1	kum_01D0	hun115_35C3	hun_01D0	esp_06D0
34				pocn15_01D1	ljo_04D0	ice_01D0	hun082_35C3	gmi_01D0
35				pocn20_01D1	maa_02D0	izo_01D0	hun115_35C3	hat_20C0
36				pocn30_01D1	mhd_01D0	jbn_29C0	ice_01D0	hba_01D0
37				pocs05_01D1	mid_01D0	key_01D0	izo_01D0	hun_01D0
38				pocs10_01D1	mlo_01C0	kum_01D0	jbn_29C0	hun115_35C3
39				pocs15_01D1	mlo_01D0	lef_01D0	key_01D0	ice_01D0
40				psa_01D0	mlo_02D0	maa_02D0	kum_01D0	izo_01D0
41				rpb_01D0	mlo_04D0	mhd_01D0	lef_01D0	izo_27C0
42				ryo_19C0	mqa_02D0	mhdcbc_11C0	lmp_28D0	jbn_29C0
43				sch_23C0	nwr_01D0	mhdrbc_11C0	maa_02D0	key_01D0
44				sey_01D0	poc000_01D1	mid_01D0	mhd_01D0	kum_01D0
45				shm_01D0	pocn05_01D1	mlo_01C0	mhdcbc_11C0	kum_04D0
46				smo_01C0	pocn10_01D1	mlo_01D0	mhdrbc_11C0	lef011_01C3
47				smo_01D0	pocn15_01D1	mlo_02D0	mid_01D0	lef_01D0
48				spo_01C0	pocn20_01D1	mnm_19C0	mlo_01C0	lef030_01C3
49				spo_01D0	pocn25_01D1	mqa_02D0	mlo_01D0	lef076_01C3
50				spo_02D0	pocn30_01D1	nwr_01D0	mlo_02D0	lef244_01C3
51				stm_01D0	pocs05_01D1	poc000_01D1	mnm_19C0	lef396_01C3
52				stmebc_01D0	pocs10_01D1	pocn15_01D1	mqa_02D0	ljo_04D0
53				syo_01D0	pocs15_01D1	pocn20_01D1	nwr_01D0	lmp_28D0
54				syo_09C0	pocs25_01D1	pocs05_01D1	poc000_01D1	maa_02D0
55				tap_01D0	pocs30_01D1	pocs15_01D1	pocn05_01D1	mhd_01D0
56				uum_01D0	pocs35_01D1	prs_21C0	pocn15_01D1	mhdcbc_11C0
57				wlg_01D0	prs_21D0	psa_01D0	pocn20_01D1	mhdrbc_11C0
58					psa_01D0	rpb_01D0	pocs05_01D1	mid_01D0
59					rpb_01D0	ryo_19C0	pocs15_01D1	mlo_01C0
60					ryo_19C0	sch_23C0	prs_21C0	mlo_01D0
61					sch_23C0	sey_01D0	psa_01D0	mlo_02D0
62					sey_01D0	shm_01D0	rpb_01D0	mlo_04D0
63					shm_01D0	sis_02D0	ryo_19C0	mnm_19C0
64					smo_01C0	smo_01C0	sch_23C0	mqa_02D0
65					smo_01D0	smo_01D0	sey_01D0	nwr_01D0
66					spo_01C0	spo_01C0	shm_01D0	prs_21C0
67					spo_01D0	spo_01D0	sis_02D0	psa_01D0
68					spo_02D0	spo_02D0	smo_01C0	rpb_01D0

Table 1. (continued)

	80-05	80-97	80-90	90-05	90-99	93-05	95-05	95-01
Site #	24	27	30	57	75	89	95	102
69					stm_01D0	stm_01D0	smo_01D0	ryo_19C0
70					stmebc_01D0	stmebc_01D0	spo_01C0	sch_23C0
71					syo_01D0	syo_01D0	spo_01D0	sey_01D0
72					syo_09C0	syo_09C0	spo_02D0	shm_01D0
73					tap_01D0	tap_01D0	stm_01D0	smo_01C0
74					uum_01D0	uta_01D0	stmebc_01D0	smo_01D0
75					wlg_01D0	uum_01D0	syo_01D0	smo_04D0
76						wlg_01D0	syo_09C0	spo_01C0
77						wlg_33C0	tap_01D0	spo_01D0
78						wpo000_10D2	uta_01D0	spo_02D0
79						wpon05_10D2	uum_01D0	spo_04D0
80						wpon10_10D2	wis_01D0	stm_01D0
81						wpon15_10D2	wlg_01D0	stmebc_01D0
82						wpon20_10D2	wlg_33C0	syo_01D0
83						wpon25_10D2	wpo000_10D2	syo_09C0
84						wpon30_10D2	wpon05_10D2	tap_01D0
85						wpos05_10D2	wpon10_10D2	tdf_01D0
86						wpos10_10D2	wpon15_10D2	uta_01D0
87						wpos15_10D2	wpon20_10D2	uum_01D0
88						wpos20_10D2	wpon25_10D2	wes_23C0
89						zep_01D0	wpon30_10D2	wis_01D0
90							wpos05_10D2	wpo000_10D2
91							wpos10_10D2	wpon05_10D2
92							wpos15_10D2	wpon10_10D2
93							wpos20_10D2	wpon15_10D2
94							yon_19C0	wpon20_10D2
95							zep_01D0	wpon25_10D2
96								wpon30_10D2
97								wpos05_10D2
98								wpos10_10D2
99								wpos15_10D2
100								wpos20_10D2
101								wpos25_10D2
102								zep_01D0

See *GlobalView* [2006] for a complete description of the individual station codes.

[a]The site names contain the following elements: [3 character site name] [data grouping]_[lab #] [sampling strategy] [sampling platform] where the "data grouping" provides a height or lat/lon; the "lab #" refers to the specific measurement laboratory; the "sampling strategy" refers to discrete (D), continuous/quasi-continuous (C), or integrated sampling (I); the "sampling platform" refers to fixed (0), ship (1), aircraft (2), tower (3), kite (4), balloon (5), or Firn/ice core (6).

[b]CO_2 observations at Darwin, Australia were excluded from consideration. See *Gurney et al.* [2004] and *Law et al.* [2003] for a discussion.

time of station introduction, a phenomenon avoided with the batch inversion method employed in this study.

[18] Three criteria were employed to arrive at the observing network makeup. First, in order to be included in a network, a station could not have more than a certain number of contiguous years in which the proportion of real to total data falls below 50%. For networks spanning more than 15 years, a station could not have more than 3 contiguous years under this criteria. For networks spanning lengths of 10 to 15 years, this number falls to no more than two. For networks spanning less than 10 years, this falls to no more than one. Second, the multi-year mean percentage of non-missing data in the years that qualified under the first criteria had to exceed 67%. Finally, no networks were begun after 1995 because of the limitation that would place on the length of available CO_2 observations and because a network starting at a later date posed few differences from those begun in 1995.

[19] The combination of these three criteria naturally led to the networks represented in Table 1. The smallest network spanning the beginning of 1979 to the end of 2005 time period contained 24 stations while the largest, spanning the beginning of 1995 to the end of 2001 time period, contained 102. The 24 station and 102 station networks are shown in Figure 1.

[20] The construction of the prior observational data covariance matrix, C(D), for the eight observational networks and its scaling to account for model-data mismatch errors followed the methodology outlined in *Baker et al.* [2006] except that, in the current study, measurements considered coincident in space and time were retained and their uncertainty was increased by the square root of the number of coincident measurements. Observing locations were considered coincident provided their latitude and longitude were within 4° of each other and they were within 900 meters in the vertical.

[21] Because of the extended time period examined, updated fossil fuel emissions were used in this study and are derived from the work of *Andres et al.* [1996], *Brenkert* [1998] and *Marland et al.* [2006]. The global fossil fuel CO_2 emissions for 2004 and 2005 were estimated using linear extrapolation of the 1998 to 2003 time period. This approach was chosen because these years exhibited consistent growth at a rate greater than previous years which,
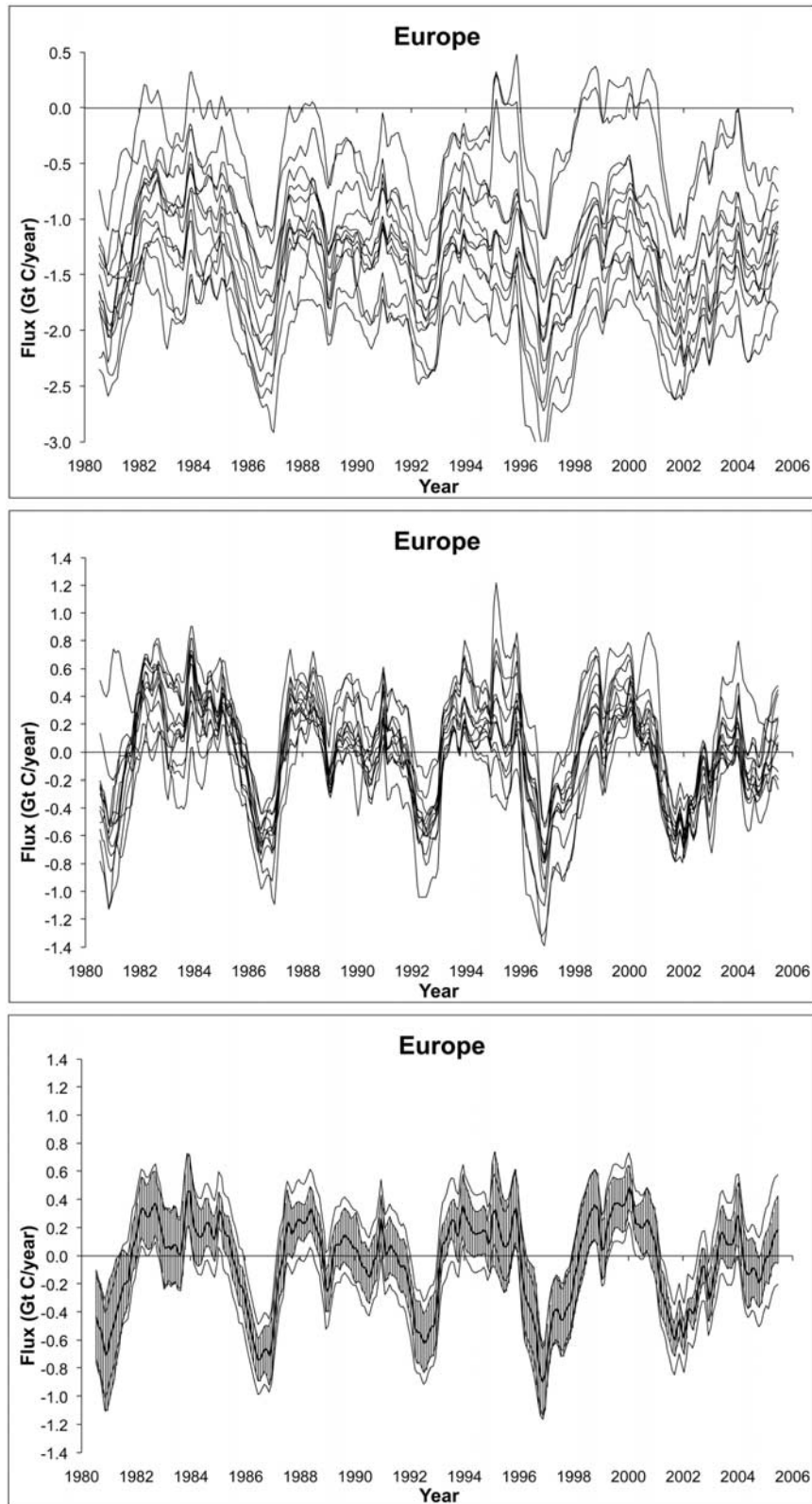
Figure 1. (a) Deseasonalized monthly net carbon exchange estimates $D_r(t)$ (GtC/year) for the Europe land region for all of the 13 participating TransCom 3 Level 2 models; (b) as in (a) but with each individual model's long-term mean (1980–2005) mean subtracted off; (c) the 13-model mean of the monthly flux estimates from (b), bounded by the 1σ within uncertainty (outer interval) and the adjusted model spread (inner hatched interval).

combined with the continued recent global economic expansion, were considered a better representation of emissions in the 2004/2005 timeframe.

2.2. Reduction of Inversion Results

[22] In order to analyze the interannual variability from the TransCom 3 inversion results, the neutral biosphere and background ocean fluxes were added back into the 11 land and 11 ocean residual fluxes returned by the inversion. This total flux represents all surface exchange other than the background fossil fuel CO_2 emissions. The individual model monthly flux estimates are then deseasonalized using a compact 13 month trapezoidal running mean as follows:

$$D_r(t) = \frac{0.5}{12} S_r(t-6) + \frac{1}{12} \sum_{t-5}^{t+5} S_r(t_i) + \frac{0.5}{12} S_r(t+6) \quad (3)$$

where $D_r(t)$ is the deseasonalized flux for a particular region, r, for a particular month, t, and $F_r(t)$ is the original flux. Though the interannual variability exhibits some model-to-model variation, the dominant difference is due to a long-term mean offset. This was shown in Figure 2 of *Baker et al.* [2006]. These offsets can be removed by computing the individual model long-term mean and removing this from every monthly flux for that model. Finally, the model mean flux estimate can be calculated in an effort to quantify the mean flux for a given month and flux region across all transport realizations in the TransCom 3 experiment.

[23] Uncertainty associated with the model mean month flux estimate is represented by the "within" uncertainty and "model spread" described in equations 1 and 2 of *Gurney et al.* [2004]. In order to compute the deseasonalized within model uncertainty, the posterior covariance matrix must be operated on by a deseasonalization operator. This is done as follows:

$$\mathbf{Q} = \mathbf{OPO}^T \quad (4)$$

where $\mathbf{Q}$ represents the deseasonalized posterior covariance matrix for an individual region and model, $\mathbf{O}$ represents the matrix form of the 13 month trapezoidal running mean, and $\mathbf{P}$ is the posterior covariance matrix for an individual region and model. An RMS operator is then applied to the diagonal of $\mathbf{Q}$ so that the within uncertainty can now be written as,

$$\overline{C\left(\overrightarrow{S}\right)} = \sqrt{\left.\sum_{n=1}^{N_{models}} Diag(\mathbf{Q}_n)\right/ N_{models}} \quad (5)$$

[24] The model spread of the deseasonalized fluxes is computed as in *Gurney et al.* [2004] except the flux, in the current case, is the deseasonalized rather than the fully seasonal flux. This can be expressed as,

$$\sigma\left(\overrightarrow{S}\right) = \sqrt{\left.\sum_{n=1}^{N_{models}} \left(\overrightarrow{S} - \overline{\left(\overrightarrow{S}\right)}_n\right)^2\right/ N_{models}} \quad (6)$$

As was shown in *Baker et al.* [2006], much of the spread across the models is due to long-term mean offsets and hence a model spread that includes a correction for the long-term mean offsets has been employed here. This was performed by computing an individual long-term mean estimated flux (spanning entire network time period) for each model/network relative to the ensemble model-mean estimate flux for that network and subtracting that offset from each monthly estimated flux for the particular model/network. This expression of model spread focuses on differences in variability rather than long-term means and, as such, is often a more appropriate measure of model-to-model variations. It is referred to throughout this study as the "adjusted model spread". An example of this is shown in Figure 1 for the Europe land region.

3. Results

[25] Figure 2 reveals how sparse the CO_2 observations can be, particularly across the tropical latitudes and in some of the TransCom land regions, such as Africa and South America. Though the networks that span the later time periods have greater station density over land, large gaps remain. This forms the core motivation for adding the prior constraint (S_0 in equation (1)) in the inversion [*Enting*, 2002]. Aggregating the regional fluxes in space and time, post-inversion, is one way to lower the uncertainty due to the limited observational constraint [*Kaminski et al.*, 2001; *Engelen et al.*, 2002]. Figure 3 shows the result of aggregating the basis function regions for total land, ocean and latitudinal totals.

3.1. Aggregated Results

[26] Figure 3a shows the model mean Total Land, Total Ocean and Global Total fluxes for the longest of the observational networks constructed in this study (1980 to 2005—24 stations). Both the within uncertainty and adjusted model spread are included. Also included in the figure is the Multivariate ENSO Index (MEI) [*Wolter and Timlin*, 1993, 1998]. The MEI is based on the six main observed variables over the Tropical Pacific and includes sea-level pressure, zonal and meridional surface winds, sea surface temperature, surface air temperature, and total cloudiness fraction. Positive values reflect the warm phase (El Niño) and are associated with warm surface water and air temperatures in the Eastern Tropical Pacific [*Trenberth and Tepaniak*, 2001].

[27] The Global Total carbon exchange variability is driven primarily by terrestrial exchange and shows a strong correlation to the ENSO timing, as has been noted by other investigators [*Bacastow*, 1976; *Keeling et al.*, 1995; *Bousquet et al.*, 2000; *Rayner et al.*, 1999b; *Feely et al.*, 1999; *Rödenbeck et al.*, 2003b; *Peylin et al.*, 2005 among others]. The Total Land carbon exchange tends to lag somewhat behind the peak of the MEI index and responds by turning from sink to source or a lessened sink. Furthermore, the influence of the June 1991 Pinatubo eruptions can be seen as a gradual strengthening of the global sink in the early 1990s, confounding the ENSO events of the early 1990s [*Bousquet et al.*, 2000].
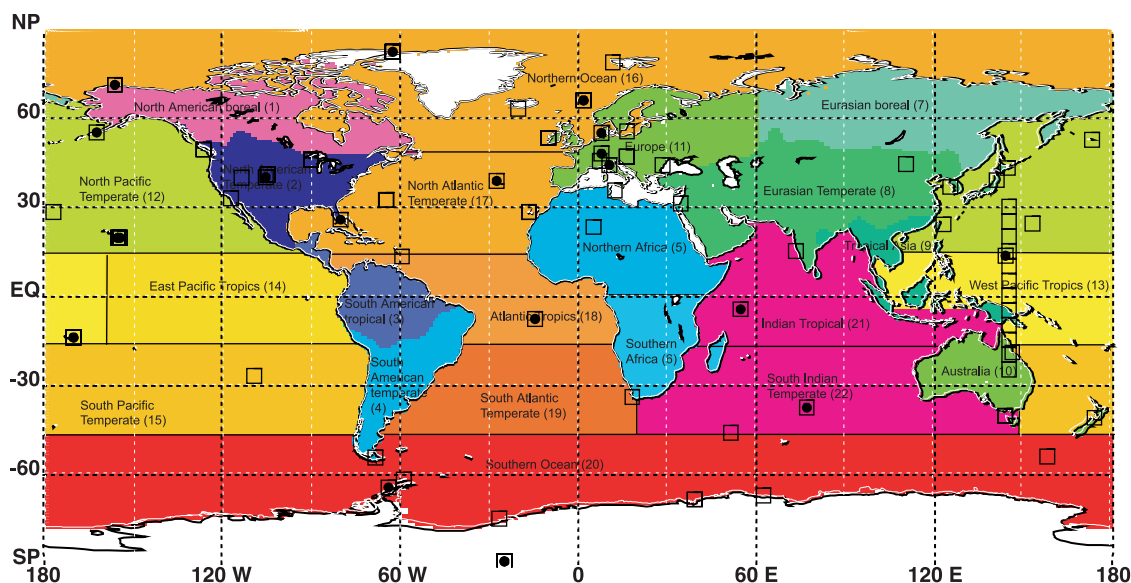
Figure 2. The locations of the observing stations for the largest (102 stations spanning 1995 to 2001—open square) and the smallest (24 stations spanning 1980 to 2005—closed circle) networks considered in this study. The 11 land and 11 ocean regions of the TransCom 3 experiment are also shown.

[28] As found in *Baker et al.* [2006], the relative magnitude of the Total Land and Total Ocean interannual variability is partly due to the tighter prior flux uncertainty of the oceans compared to the land. However, experiments in which the ocean prior flux uncertainty was scaled to closely match the average level over the land regions show that the relative amounts of interannual variability are not completely dependent upon the prior uncertainty, but reflect constraints imposed by the observed CO_2. The ratio of Total Ocean to Total Land 1σ variability in the 1980–2005 observational network with commensurate prior flux uncertainties was 0.8 (compared to 0.31 for the "non-loosened" prior uncertainties) while the same ratio, when the inversion is performed with the 1995 to 2001 observational network, is 0.68 (compared to 0.40 in the "non-loosened" case). The tighter ocean prior flux uncertainties have an influence on the relative land/ocean variability, but that influence lessens as more observing stations are included in the inverse setup.

[29] Figures 3b and 3c show the ocean and land regions divided into north, tropical and southern domains. On land, the Southern Land and Tropical Land aggregated regions exhibit slightly more interannual variability than the Northern Land region. In this study, the Southern Land includes the Southern Africa region and this accounts for much of the variability in the Southern Land region. In the ocean, the Tropical Ocean aggregate region exhibits the greatest variability. In both the land and ocean aggregated regions, the within uncertainty in the tropics is larger than the adjusted model spread. This, in turn, is driven by the limited number of observations in the tropical regions, particularly over land, and the fact that rapid vertical mixing limits the constraint imposed by surface observations [*Baker et al.*, 2006]. As will be shown later, this is improved somewhat by networks that include observing stations added in the 1990s and the first part of the 21st century.

[30] The adjusted model spread in the flux estimation across the models is much smaller than the within uncertainty in all of the aggregated regions—this is primarily due to the fact that the spread has been constructed by removing the individual model long-term mean offsets. The dominance of the within error is a persistent theme throughout the analysis and suggests that the models agree on the

Figure 3. TransCom 3 Level 2 model mean deseasonalized net carbon exchange estimated using the 24-station 1980 to 2005 observational network. (a) Total Land (thick red line), Total Ocean (thick blue line) and Global Total (thick black line) fluxes. (b) Northern Land (solid black line; sum of Boreal N America, Temperate N America, Boreal Asia, Temperate Asia, Europe), Tropical Land (solid red line; sum of Tropical America, Northern Africa, Tropical Asia), and Southern Land (solid blue line; sum of South America, Southern Africa, Australasia) fluxes. (c) Northern Oceans (solid black line; sum of Northern Pacific, Northern Ocean, North Atlantic), Tropical Oceans (solid red line; sum of East Pacific, West Pacific, Tropical Atlantic, Tropical Indian), and Southern Oceans (solid blue line; sum of South Pacific, Southern Ocean, South Atlantic, South Indian) fluxes. Within uncertainty interval (1σ) is shown by thin solid lines and the adjusted model spread by the hatched interval. Note the two y-axes in each plot and the shifted scales for each. Also shown in (a) (thick green line) is the Multivariate El Niño/Southern Oscillation (ENSO) Index (MEI) [*Wolter and Timlin*, 1993, 1998], as well as the timing of the Mt. Pinatubo eruption.
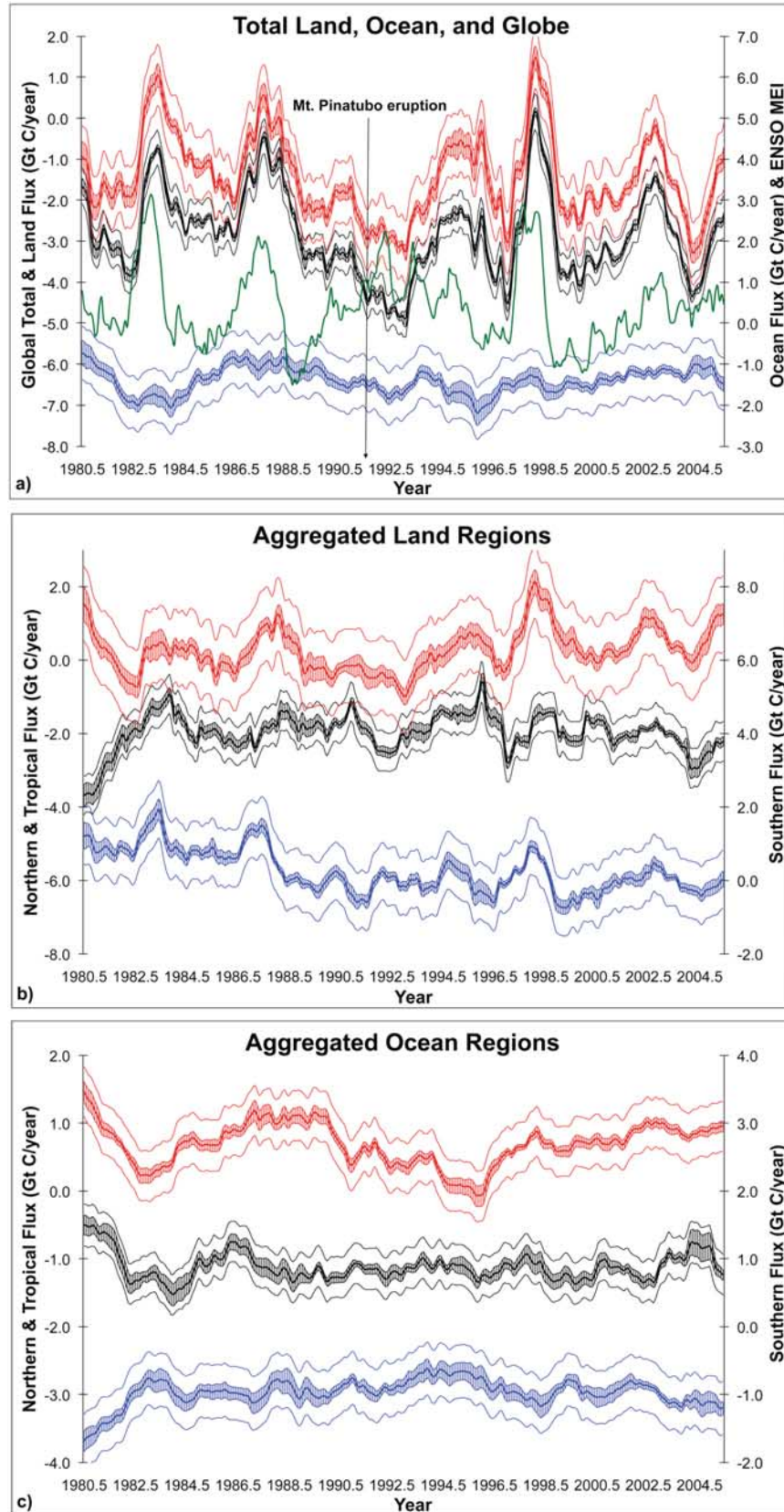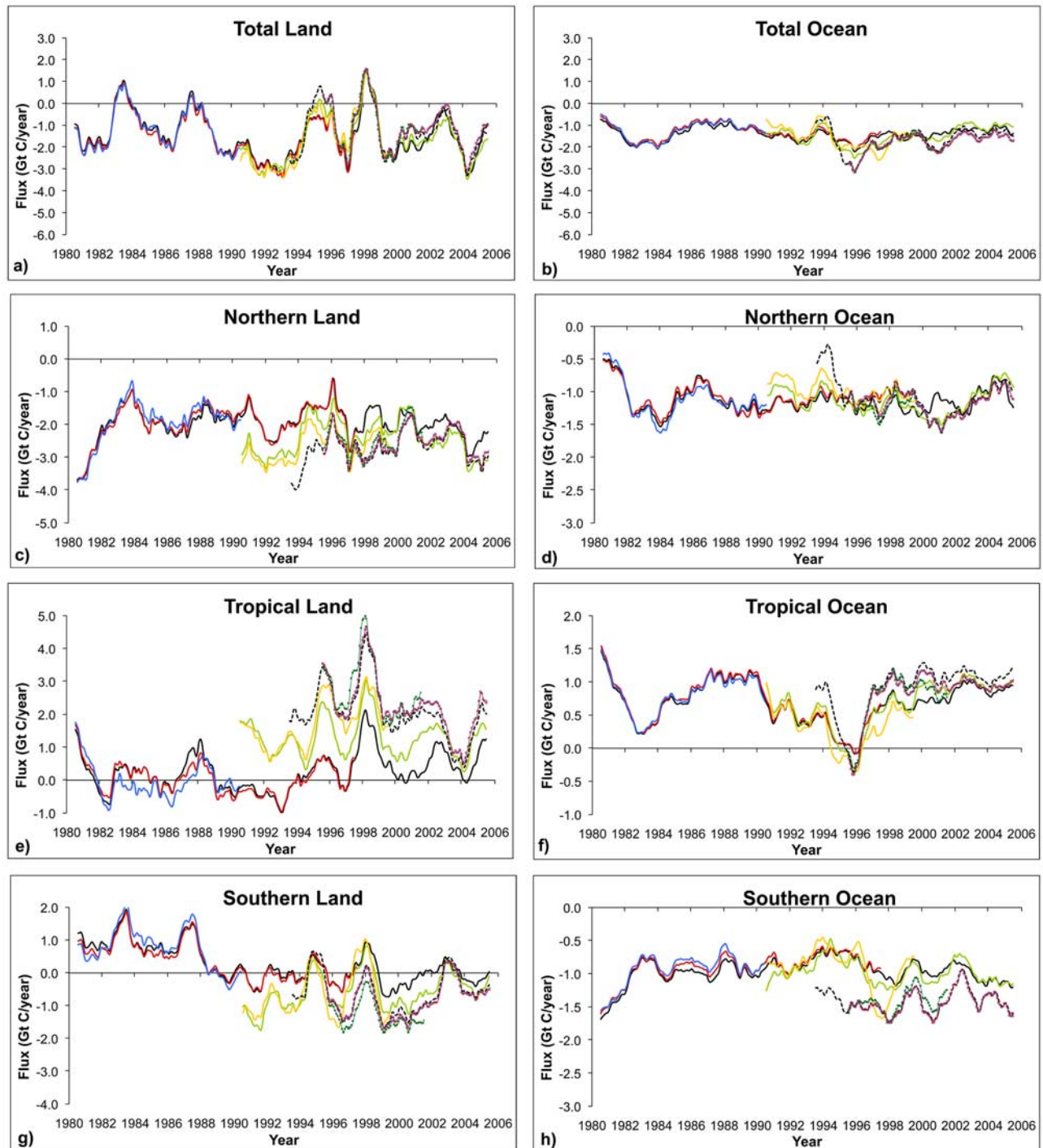
Figure 3

Figure 4. TransCom 3 Level 2 model mean deseasonalized net carbon exchange estimated for latitudinal aggregates (as defined in caption to Figure 3) using all eight observational networks (see Table 1): 1980–2005; 24 stations (black solid), 1980–1997; 27 stations (red solid), 1980–1990; 30 stations (blue solid), 1990–2005; 57 stations (green solid), 1990–1999; 75 stations (gold solid), 1993–2005; 89 stations (black dashed), 1995–2001; 102 stations (green with diamond symbol), 1995–2005; 95 stations (lavender with square symbol). (a) Total Land; (b) Total Ocean; (c) Northern Land; (d) Northern Oceans; (e) Tropical Land; (f) Tropical Oceans; (g) Southern Land; (h) Southern Oceans.
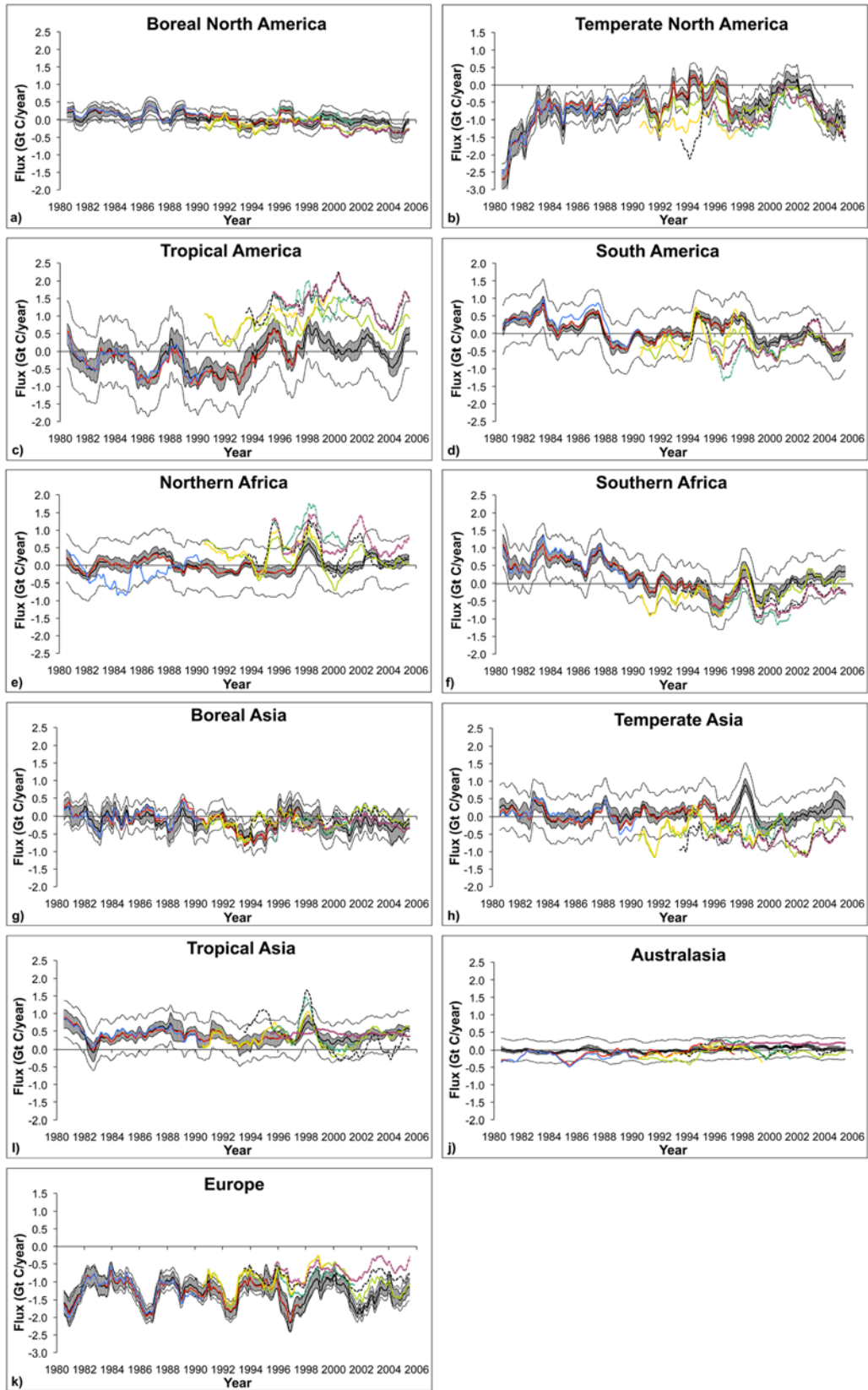
Figure 5

interannual variations to a much greater extent than found with the estimation of long-term means. Other studies have arrived at similar conclusions, whether considering a transport model suite as in *Baker et al.* [2006] or a range of inversion parameters [*Bousquet et al.*, 2000; *Peylin et al.*, 2005].

3.2. Observing Network Influence

[31] The influence of using different observing networks can be seen in Figure 4, which presents the global total and latitudinal aggregates for the entire time period and with all observing networks. For the Total Land and Total Ocean, both the long-term means and the interannual variations show considerable agreement. As noted before, the larger (and hence shorter timespan) networks differ in size (number of stations) from one another to a greater degree than the smaller networks. Furthermore, these stations contain a higher proportion of continental versus ocean sites and hence pose greater challenges to model transport [*Patra et al.*, 2006]. Not surprisingly, inter-network differences are much greater in the 1990s and the early years of the 21st century.

[32] The agreement between the observing networks in the latitudinal aggregates is much less but is primarily composed of constant long-term offsets and amplitude differences. Much of the phasing of the variability remains coherent across the networks. Exceptions to this are the 1990 to 1995 period in the Tropical Land region where the networks that begin in 1990 (57 and 75 stations) show features nearly opposite in sign to those in the longer networks (24 and 27). The Northern Ocean shows a similar feature in the 2000 to 2002 time period. Other notable phase mismatches occur in the Northern Land and the Southern Ocean, 1997 to 1999.

[33] Figure 5 presents the model mean, deseasonalized carbon exchange for all of the individual land and ocean regions and for all observing networks. The within uncertainty and the adjusted model spread associated with the longest-running observing network (1980 to 2005) are included in the figure. It is worth noting that the adjusted model spread in the longest-running observing network reflects the model-to-model differences with long-term means removed but the model mean flux for the remaining networks contain long-term mean offsets.

[34] Many regions show significant differences in both the long-term mean flux and flux variations across the different station networks. Long-term mean flux offsets are notable in Tropical America and Northern Africa, with the smaller networks showing net emission of over 1.0 GtC/year versus the larger networks which show a near-neutral net exchange. Similarly, the shorter networks show net

uptake in Temperate Asia across the decades of the 1990s and 2000s whereas the longer networks show near neutral exchange. The smaller networks show a somewhat weaker uptake over the 1990s and 2000s in Europe relative to the longer observing networks, which estimate uptake of roughly 1.5 GtC/year. In the ocean regions, the South Pacific ocean shows large long-term mean flux discrepancies (>1 GtC/year) from one network to the other in the 1990s and 2000s. The South Atlantic ocean and Southern Ocean show discrepancies in the mid- to late-1990s while the North Atlantic ocean shows some discrepancies in the 1980s.

[35] Though network dependence does occur, the phasing of the flux variability is often consistent across station networks even when the amplitude is not. Examples of this include Temperate North America, Southern Africa, Europe, the Pacific and Indian oceans.

[36] On land, the interannual variability is consistently greatest in the Temperate North America and Tropical America land regions. In the oceans, the South Pacific ocean and Tropical Indian ocean tend to dominate the interannual variability. The Tropical America land region exhibits shifts of almost 2 GtC/year over the course of 2 to 3 years, while the Tropical Indian ocean region exhibits variations as large as 1 GtC/year over a 2-year timespan.

[37] The two uncertainties vary in a relative sense from region to region. Overall, the 1σ within uncertainties are larger than the 1σ model spread (true for both original and adjusted form). Exceptions to this occur in Europe and particular time periods in Temperate North America and the Northern Ocean regions. In these few cases, flux differences among the individual models are as large as the average of individual model error. Furthermore, the magnitude of the model spread often varies over time, suggesting that disagreement between model estimated fluxes is more pronounced at times.

[38] Another way of examining the dependence of the uncertainty estimates on the network size is presented in Figure 6. For each of the eight networks, the within uncertainty and model spread were computed based on the first 5 years of error covariances and fluxes. As the station network increases in size, the overall observational constraint increases, causing the within uncertainty to decline. However, the increase in network size has the opposing influence on the model spread, causing it to increase. The decline in the within uncertainty reflects the increasing observational constraint placed on the flux estimates. The rise in the model spread, however, reflects the fact that as stations are added to the observing network, the differences between the models are systematically exposed to a greater degree. The model spread is also consistently larger over the land regions than over the ocean. This is due

---

Figure 5. TransCom 3 Level 2 net carbon exchange estimated for individual regions using all eight observational networks (as defined in caption to Figure 4). (a) Boreal N America. (b) Temperate N America. (c) Tropical America. (d) South America. (e) Northern Africa. (f) Southern Africa. (g) Boreal Asia. (h) Temperate Asia. i) Tropical Asia. (j) Australasia. (k) Europe. (l) North Pacific. (m) West Pacific. (n) East Pacific. (o) South Pacific. (p) Northern Ocean. (q) North Atlantic. (r) Tropical Atlantic. (s) South Atlantic. (t) Southern Ocean. (u) Tropical Indian. (v) South Indian. Within uncertainty interval (1σ) is shown by thin black solid lines and the adjusted model spread by the hatched interval for the longest observational network only (1980–2005; 24 stations). Note that the vertical scale is different for the land versus ocean regions.
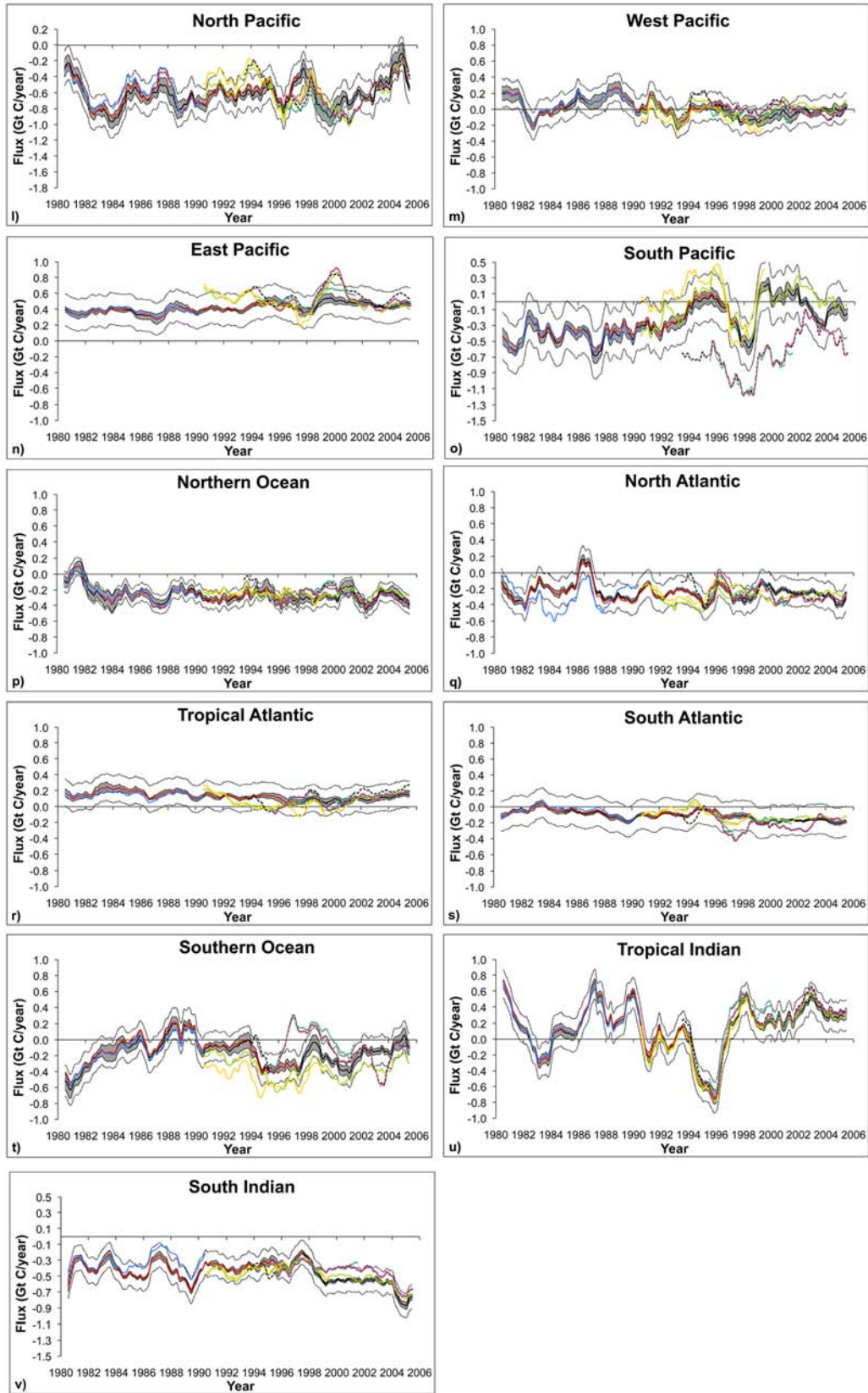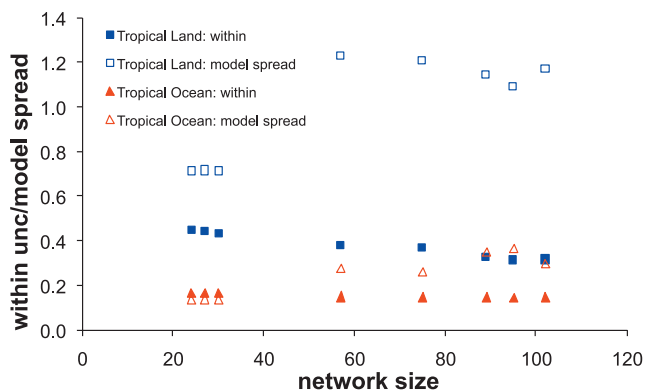
Figure 5. (continued)

Figure 6. Network within uncertainty and model spread for the aggregate Tropical Land region (sum of Tropical America, Northern Africa, Tropical Asia) based on the first 5 years of net carbon exchange covariances (within uncertainty) and fluxes (model spread) for each of the eight observing networks (as defined in caption to Figure 4). The within uncertainty calculation was computed from the full posterior covariance matrices according to equation (5).

to the limited number of observing sites in tropical land regions and the fact that CO_2 gradients over land are larger and more dependent upon differences in transport out of the planetary boundary layer [*Gurney et al.*, 2003].

4. Discussion

[39] As expected, the interannual variations in the net terrestrial carbon exchange at the global scale are consistent with a number of other inverse studies that quantified interannual variations [*Bousquet et al.*, 2000; *Rödenbeck*

et al., 2003b; *Patra et al.*, 2005; *Rayner et al.*, 2005; *Peylin et al.*, 2005; *Baker et al.*, 2006]. All show correspondence between land fluxes and the El Niño/Southern Oscillation. In addition, all these studies show a reduction in the ENSO-flux correlation for the period following the Mt. Pinatubo eruption in the Philippines, in which large amounts of aerosol were emitted into the stratosphere and subsequently transported around the planet. Beyond cancellation of the positive carbon flux anomaly associated with the ENSO timing, the period following the Pinatubo eruption is marked by a gradual increase in uptake on land. This negative flux anomaly is most readily seen in the Boreal Asia, Temperate North America, Tropical Asia, and Europe regions (see Figure 5). Negative anomalies are also evident in the Tropical America and Temperate Asia regions for the shorter networks suggesting that the post-Pinatubo impact was felt widely across both the tropical and northern extratropical land regions. This has been hypothesized as NPP stimulation from the increase in diffuse to direct radiation resulting from the aerosol loading in the atmosphere [*Gu et al.*, 2003; *Farquhar and Roderick*, 2003]. Recent modeling research suggests that, rather than an NPP stimulation, the decline in the CO_2 atmospheric growth rate results from a combination of greater ocean uptake, reduced heterotrophic respiration, and reduced biomass burning [*Angert et al.*, 2004].

[40] Results from *Peylin et al.* [2005] show the inverse result placing most of the negative anomaly in North America but the biogeochemical model simulations also performed in that study show a somewhat broader anomaly across the northern hemisphere. *Rödenbeck et al.* [2003b] place the negative anomaly in Tropical America and the eastern portion of Temperate North America.
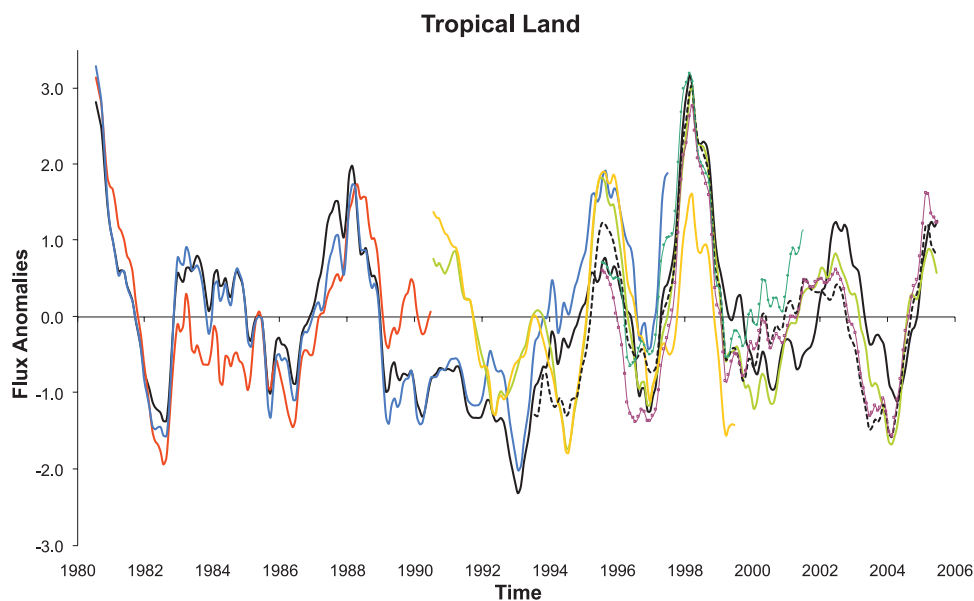
Figure 7. TransCom 3 Level 2 model mean Tropical Land net carbon exchange anomalies for all eight observational networks (as defined in caption to Figure 4). Fluxes have been deseasonalized, detrended (monthly fluxes adjusted by the long-term mean slope to achieve a long-term mean slope of zero), standardized (anomalies are in units of standard deviation), and long-term means are centered on zero flux.

[41] The most obvious example of the relationship between ENSO and net carbon exchange can be seen for the very strong ENSO event of 1997/1998. Large biomass fires in Tropical Asia were related to this ENSO event; one study estimated the carbon loss during this period to range from 0.8 to 2.6 GtC/year, while another had a larger upper bound estimating losses at 0.8 to 3.7 GtC/year [*Page et al.*, 2002; *Langenfelds et al.*, 2002; *van der Werf et al.*, 2006]. All are consistent with the TransCom results, which show a positive flux anomaly during this period [*Schimel and Baker*, 2002; *Baker et al.*, 2006].

[42] The magnitude of this global land flux anomaly evident in Figure 3 is roughly 4.0 GtC/year. This anomaly is seen in the aggregated Tropical Land region estimate, totaling roughly 2 to 2.5 GtC/year, and in the Southern Land region total at approximately 1.0 to 1.5 GtC/year. Though the eight networks show mean offsets, the anomalous flux is consistent in terms of phasing and magnitude, as shown by the normalization of the Tropical Land flux anomalies in Figure 7.

[43] Recent work by *van der Werf et al.* [2006] on fire events shows significant consistency with some of the larger flux anomalies in the Tropical Land and Southern Land regions. Roughly two thirds of the 1997 global carbon emissions due to fire were attributed in that study to a region similar to the Tropical Asia region in this study (Figure 5i). The remainder of fire-derived carbon emissions in 1997 were attributed to regions closely aligned with the Southern Africa and South America regions denoted here (Figures 5f and 5d, respectively). The 1997 ENSO anomaly is also evident in the inverse estimated fluxes for the Temperate Asia region, though this flux anomaly disappears for networks composed of greater than 30 stations. These same larger networks show a larger positive flux anomaly for the Tropical Asia region then, raising the possibility that the smaller networks have insufficient information to separate the fluxes in these two neighboring flux regions. No significant fire emissions are evident in *van der Werf et al.* [2006] for the Temperate Asia region.

[44] The station networks that extend back to 1980 allow for an analysis of previous ENSO events. The Southern Land aggregate region shows positive flux anomalies in both the 1982/1983 and 1987 ENSO events, while the Tropical Land shows a response for the 1987 ENSO only, driven solely by Tropical America (though somewhat lagged). Unlike the strong 1997/1998 ENSO event, the Tropical Asia region shows little response to the earlier ENSO events. South America and Southern Africa exhibit positive flux anomalies coincident with all three large ENSO events among the southern land regions. Temperate Asia also shows a positive anomaly during these earlier ENSO events though the fact that the larger networks eliminated the response in 97/98 raises questions about how well the sparser networks are able to separately estimate fluxes at the continental scale. *Rödenbeck et al.* [2003b] also found little response in Tropical Asia to the ENSO events of the 1980s, while showing a large positive flux response to the 1997/1998 event.

[45] The strong ENSO event of 1997/1998 was also observed to cause lessened outgassing of CO_2 from the

Eastern Tropical Pacific and has been estimated in some of the inverse studies [*Feely et al.*, 2002; *Patra et al.*, 2005; *Peylin et al.*, 2005]. Like the study of *Baker et al.* [2006], this study finds an anomalous uptake in the Eastern Tropical Pacific ($\sim$0.2 GtC/year) and a larger anomalous uptake in the South Pacific region ($\sim$0.6 GtC/year).

[46] Consistent among most of the interannual inverse studies is the conclusion that the interannual variability in the global exchange is dominated by the land versus the ocean [*Bousquet et al.*, 2000; *Rödenbeck et al.*, 2003b; *Patra et al.*, 2005; *Baker et al.*, 2006; *Peylin et al.*, 2005]. Furthermore, the oceanic interannual variability is greatest in the tropics, though large variability can be found in the Southern Ocean and South Pacific. Tropical ocean variability is dominated by the Tropical Indian ocean. As mentioned previously, the lesser ocean versus land interannual variability can partly be explained by the tighter ocean prior flux uncertainty, though as the observational constraint increases with increasing observing network size, the lesser ocean variability appears to be a reflection of the observational data constraint.

5. Conclusions

[47] The TransCom 3 Level 2 experiment is an atmospheric CO_2 inversion in which 13 participating modeling groups submitted atmospheric CO_2 concentration flux responses to which the inverse method has been applied. In the current study, the TransCom 3 interannual inversion has been extended to span the 1980 to 2005 time period. In addition to examining the estimation uncertainty and spread of results from the participating modeling groups, this study has also examined the sensitivity of the results to eight different observing networks. Constructing different networks allows us to examine earlier time periods in which fewer sites were taking data, while avoiding potential time-dependent biases associated with varying the sites used inside a single inversion.

[48] The results of this research confirm that the land is the dominant contributor to the interannual variability in the net carbon exchange: the inversions for all the station networks exhibit this broad feature. In both the ocean and land, the tropics tend to account for the majority of the interannual variability.

[49] As has been found in previous work, the total land net carbon exchange shows considerable correlation with the El Niño/Southern Oscillation, with positive terrestrial carbon flux anomalies coinciding with the peak of the ENSO warm phase. The large 1997/1998 ENSO event is easily discerned and is seen most clearly in the carbon flux estimates for the Tropical Asia, Temperate Asia, Northern Africa and Southern Africa land regions. The carbon emission during this period is consistent with the observation of large fires in Tropical Asia. Earlier ENSO events of the 1980s are most evident in southern land positive flux anomalies, particularly evident in South America and Southern Africa.

[50] The slowing of the global CO_2 growth rate after the Pinatubo eruption is also evident in the Total Land net carbon exchange and this appears to be evident at the

regional scale over much of the tropical and northern extratropical land regions. The within uncertainty remains greatest in the tropics but lessens as additional observing stations are included in the station networks. The model spread, however, increases with increasing station density, owing to the greater observational constraint illuminating the model-to-model transport differences.

[51] Consideration of the interannual variability shows that the phasing of the flux variability is relatively consistent across model transport and the eight networks, particularly for the latitudinally aggregated land and ocean regions. This consistency is somewhat less when the 22 individual basis function regions are considered. However, even at the individual basis function region, inconsistencies are for particular isolated timespans only.

[52] The consistency of the results among the station networks in terms of the interannual variability suggests that these time-dependent inversions could be used to explore the relationships between net carbon exchange and climate indices or climate variability itself. Such an exploration may hold insights into biogeochemical mechanisms and is an important consideration for future research.

[53] Though the participating models in the TransCom 3 experiment show considerable agreement on the interannual variations in net carbon exchange, further exploration into the model-to-model differences remains a top priority for research, as transport is a significant contributor to the uncertainty in inverse results. Furthermore, the potential for bias in the transport algorithms of the models involved must be examined and used to improve transport simulations. This is particularly true for long-term mean flux estimation, for which uncertainties appear much greater than estimates of interannual variation.

[54] Other aspects of this work deserving of more attention include an exploration of individual station sensitivity. It is likely that a small subset of stations are responsible for most of the inconsistencies seen between the networks.

[55] Lastly, the time-dependant inversions performed here should be updated with the newly available vertical CO_2 profile measurements in order to explore how these measurements might alter both the long-term mean and the interannually-varying carbon flux estimates as has been suggested in recent research [Stephens et al., 2007].

References

Andres, R. J., G. Marland, I. Fung, and E. Matthews (1996), A $1° \times 1°$ distribution of carbon dioxide emissions from fossil fuel consumption and cement manufacture, 1950–1990, *Global Biogeochem. Cycles*, *10*(3), 419–429.

Angert, A., S. Biraud, C. Bonfils, W. Buermann, and I. Fung (2004), CO_2 seasonality indicates origins of post-Pinatubo sink, *Geophys. Res. Lett.*, *31*, L11103, doi:10.1029/2004GL019760.

Bacastow, R. B. (1976), Modulation of atmospheric carbon dioxide by the southern oscillation, *Nature*, *261*, 116–118.

Baker, D. F., et al. (2006), TransCom 3 inversion intercomparison: Impact of transport model errors on the interannual variability of regional CO_2 fluxes, 1988–2003, *Global Biogeochem. Cycles*, *20*, GB1002, doi:10.1029/2004GB002439.

Bousquet, P., P. Peylin, P. Ciais, C. Le Quéré, P. Friedlingstein, and P. Tans (2000), Regional changes in carbon dioxide fluxes of land and oceans since 1980, *Science*, *290*, 1342–1346.

Brenkert, A. L. (1998), Carbon dioxide emission estimates from fossil-fuel burning, hydraulic cement production, and gas flaring for 1995 on a one degree grid cell basis. (Available at http://cdiac.esd.ornl.gov/ndps/ndp058a.html)

Cox, P. M., R. A. Betts, C. D. Jones, S. A. Spall, and I. J. Totterdell (2000), Acceleration of global warming due to carbon-cycle feedbacks in a coupled climate model, *Nature*, *408*, 184–187.

Dargaville, R. J., R. M. Law, and F. Pribac (2000), Implications of interannual variability in atmospheric circulation on modeled CO_2 concentrations and source estimates, *Global Biogeochem. Cycles*, *14*(3), 931–943.

Engelen, R. J., A. S. Denning, and K. R. Gurney (2002), On error estimation in atmospheric CO_2 inversions, *J. Geophys. Res.*, *107*(D22), 4635, doi:10.1029/2002JD002195.

Enting, I. (2002), *Inverse Problems in Atmospheric Constituent Transport*, Cambridge Univ. Press, New York.

Enting, I. G., C. M. Trudinger, and R. J. Francey (1995), A synthesis inversion of the concentration and $\delta^{13}C$ of atmospheric CO_2, *Tellus*, *47B*, 35–52.

Fan, S., M. Gloor, J. Mahlman, S. Pacala, J. Sarmiento, T. Takahashi, and P. Tans (1998), A large terrestrial carbon sink in North America implied by atmospheric and oceanic carbon dioxide data and models, *Science*, *282*, 442–446.

Farquhar, G. D., and M. L. Roderick (2003), Atmospheric science: Pinatubo, diffuse light, and the carbon cycle, *Science*, *299*, 1997–1998.

Feely, R., R. Wanninkhof, T. Takahashi, and P. Tans (1999), Influence of El Niño on the equatorial pacific contribution to atmospheric CO_2 accumulation, *Nature*, *398*, 597–601.

Feely, R. A., et al. (2002), Seasonal and interannual variability of CO_2 in the equatorial pacific, *Deep-Sea Res. Part II*, *49*, 2443–2469.

Friedlingstein, P., et al. (2006), Climate-carbon cycle feedback analysis: Results from the C4MIP model intercomparison, *J. Clim.*, *19*, 3337–3353.

GLOBALVIEW-CO_2 (2006), Cooperative Atmospheric Data Integration Project - Carbon Dioxide, CD-ROM, NOAA CMDL, Boulder, Colorado. (Also available on Internet via anonymous FTP to ftp.cmdl.noaa.gov, Path: ccg/co2/GLOBALVIEW)

Gu, L., D. D. Baldocchi, S. C. Wofsy, J. W. Munger, S. P. Urbanski, and T. A. Boden (2003), Response of a deciduous forest to the mount Pinatubo eruption: Enhanced photosynthesis, *Science*, *299*, 2035–2038.

Gurney, K., R. Law, P. Rayner, and A. S. Denning (2000), TransCom 3 Experimental Protocol, Department of Atmospheric Science, Colorado State University, USA, Paper 707. (Available at http://transcom.colostate.edu/TransCom_3/transcom_3.html)

Gurney, K. R., et al. (2002), Towards robust regional estimates of CO_2 sources and sinks using atmospheric transport models, *Nature*, *415*, 626–630.

Gurney, K. R., et al. (2003), TransCom 3 CO_2 Inversion Intercomparison: 1. Annual mean control results and sensitivity to transport and prior flux information, *Tellus*, *55B*, 555–579.

Gurney, K. R., et al. (2004), Transcom 3 Inversion Intercomparison: Model mean results for the estimation of seasonal carbon sources and sinks, *Global Biogeochem. Cycles*, *18*, GB1010, doi:10.1029/2003GB002111.

Gurney, K. R., Y.-H. Chen, T. Maki, S. R. Kawa, A. Andrews, and Z. Zhu (2005), Sensitivity of atmospheric CO_2 inversions to seasonal and interannual variations in fossil fuel emissions, *J. Geophys. Res.*, *110*, D10308, doi:10.1029/2004JD005373.

Kaminski, T., P. J. Rayner, M. Heimann, and I. G. Enting (2001), On aggregation errors in atmospheric transport inversions, *J. Geophys. Res.*, *106*(D5), 4703–4715.

Keeling, C. D., T. P. Whorf, M. Wahlen, and J. Vanderplicht (1995), Interannual extremes in the rate of rise of atmospheric carbon-dioxide since 1980, *Nature*, *375*, 666–670.

Langenfelds, R. L., R. J. Francey, B. C. Pak, L. P. Steele, J. Lloyd, C. M. Trudinger, and C. E. Allison (2002), Interannual growth rate variations of atmospheric CO_2 and its $\delta^{13}C$, H_2, CH_4, and CO between 1992 and 1999 linked to biomass burning, *Global Biogeochem. Cycles*, *16*(3), 1048, doi:10.1029/2001GB001466.

Law, R. M., Y.-H. Chen, and K. R. Gurney (2003), TransCom 3 CO_2 inversion intercomparison: 2. Sensitivity of annual mean results to data choices, *Tellus*, *55B*, 580–595.

Marland, G., T. A. Boden, and R. J. Andres (2006), Global, Regional, and National Fossil Fuel CO2 Emissions, in *Trends: A Compendium of Data on Global Change. Carbon Dioxide Information Analysis Center*, Oak Ridge National Laboratory, U.S. Department of Energy, Oak Ridge, Tenn.

Page, S. E., F. Siegert, J. O. Rieley, H. D. V. Boehm, A. Jaya, and S. Limin (2002), The amount of carbon released from peat and forest fires in Indonesia during 1997, *Nature*, *420*, 61–65.

Patra, P. K., S. Maksyutov, and TransCom 3 Modelers (2003), Sensitivity of optimal extension of CO_2 observation networks to model transport, *Tellus*, *55B*, 498–511.

Patra, P. K., M. Ishikawa, S. Maksyutov, T. Nakazawa, and G. Inoue (2005), Role of biomass burning and climate anomalies for land-atmosphere carbon fluxes based on inverse modeling of atmospheric CO_2, *Global Biogeochem. Cycles*, *19*, GB3005, doi:10.1029/2004GB002258.

Patra, P. K., et al. (2006), Sensitivity of inverse estimation of annual mean CO_2 sources and sinks to ocean-only sites versus all-sites observational networks, *Geophys. Res. Lett.*, *33*, L05814, doi:10.1029/2005GL025403.

Peylin, P., P. Bousquet, C. Le Quéré, S. Sitch, P. Friedlingstein, G. McKinley, N. Gruber, P. Rayner, and P. Ciais (2005), Multiple constraints on regional CO_2 flux variations over land and oceans, *Global Biogeochem. Cycles*, *19*, GB1011, doi:10.1029/2003GB002214.

Prentice, I. C., G. Farquhar, M. Fashm, M. Goulden, M. Heimann, V. Jaramillo, H. Kheshgi, C. Le Quéré, and R. J. Scholes (2001), The carbon cycle and atmospheric carbon dioxide, in *Climate Change 2001: The Scientific Basis, Contribution of Working Group I to the Third Assessment Report of the Intergovernmental Panel on Climate Change*, edited by J. T. Houghton et al., pp. 183–237, Cambridge Univ. Press, New York.

Randerson, J. T., M. V. Thompson, T. J. Conway, I. Y. Fung, and C. B. Field (1997), The contribution of terrestrial sources and sinks to trends in the seasonal cycle of atmospheric carbon dioxide, *Global Biogeochem. Cycles*, *11*(4), 535–560.

Rayner, P. J., I. G. Enting, R. J. Francey, and R. L. Langenfelds (1999a), Reconstructing the recent carbon cycle from atmospheric CO_2, $\delta^{13}C$ and O_2/N_2 observations, *Tellus*, *51B*, 213–232.

Rayner, P. J., R. M. Law, and R. Dargaville (1999b), The relationship between tropical CO_2 fluxes and the El Niño-Southern Oscillation, *Geophys. Res. Lett.*, *26*(4), 493–496.

Rayner, P. J., M. Scholze, W. Knorr, T. Kaminski, R. Giering, and H. Widmann (2005), Two decades of terrestrial carbon fluxes from a carbon cycle data assimilation system (CCDAS), *Global Biogeochem. Cycles*, *19*, GB2026, doi:10.1029/2004GB002254.

Rödenbeck, C., S. Houweling, M. Gloor, and M. Heimann (2003a), Time-dependent atmospheric CO_2 inversions based on interannually varying tracer transport, *Tellus*, *55B*, 488–497.

Rödenbeck, C., S. Houweling, M. Gloor, and M. Heimann (2003b), CO_2 flux history 1982–2001 inferred from atmospheric data using a global inversion of atmospheric transport, *Atmos. Chem. Phys.*, *3*, 1919–1964.

Schimel, D., and D. Baker (2002), The wildfire factor, *Nature*, *420*, 29–30.

Stephens, B. B., et al. (2007), Weak northern and strong tropical land carbon uptake from vertical profiles of atmospheric CO_2, *Science*, *316*, 1732–1735.

Takahashi, T., R. H. Wanninkhof, R. A. Feely, R. F. Weiss, D. W. Chipman, N. Bates, J. Olafsson, C. Sabine, and S. C. Sutherland (1999), Net sea-air CO_2 flux over the global oceans: An improved estimate based on the sea-air pCO_2 difference, Proceedings of the 2nd CO_2 in Oceans Symposium, Tsukuba, Japan.

Tarantola, A. (1987), Chapter 4 in: Inverse Problem Theory: Methods for Data Fitting and Parameter Estimation, Elsevier, Amsterdam.

Trenberth, K. E., and D. P. Tepaniak (2001), Indices of El Niño evolution, *J. Clim.*, *14*, 1697–1701.

van der Werf, G. R., et al. (2006), Interannual variability in global biomass burning emissions from 1997 to 2004, *Atmos. Chem. Phys.*, *6*, 3423–3441.

Wolter, K. and M. S. Timlin (1993), Monitoring ENSO in COADS with a seasonally adjusted principal component index, *Proc. of the 17th Climate Diagnostics Workshop*, Norman, OK, NOAA/N MC/CAC, NSSL, Oklahoma Clim. Survey, CIMMS and the School of Meteor., Univ. of Oklahoma, 52–57. (Available at http://www.cdc.noaa.gov/~kew/MEI/mei.html#ref_wt1)

Wolter, K., and M. S. Timlin (1998), Measuring the strength of ENSO - How does 1997/98 rank?, *Weather*, *53*, 315–324.

————————————————

D. Baker, Woods Hole Oceanographic Institution, 266 Woods Hole Road, Woods Hole, MA 02543, USA. (dbaker@whoi.edu)

S. Denning, Department of Atmospheric Science, Colorado State University, 1371 Campus Delivery, Fort Collins, CO 80523-1371, USA. (denning@atmos.colostate.edu)

K. R. Gurney, Department of Earth and Atmospheric Sciences/Department of Agronomy, Purdue University, 550 Stadium Mall Drive, West Lafayette, IN 47907, USA. (kgurney@purdue.edu)

P. Rayner, Bat. 701 LSCE-CEA de Saclay, Orme des Merisiers, 91191 Gif/Yvette, France. (peter.rayner@cea.fr)